The Cryosphere Discussions

Seasonal speed-up of two outlet glaciers of Austfonna, Svalbard, inferred from continuous GPS measurements

T. Dunse[1], T. V. Schuler[1], J. O. Hagen[1], and C. H. Reijmer[2]

[1]Department of Geosciences, University of Oslo, P.O. Box 1047, Blindern, 0316 Oslo, Norway
[2]Institute for Marine and Atmospheric Research Utrecht, Utrecht University, Princetonplein 5, 3584 CC Utrecht, The Netherlands

Correspondence to: T. Dunse (thorben.dunse@geo.uio.no)

Title Page

Abstract	Introduction
Conclusions	References
Tables	Figures

|◄ | ►|
◄ | ►

Back | Close

Full Screen / Esc

Printer-friendly Version

Interactive Discussion

Seasonal speed-up of two outlet glaciers of Austfonna

T. Dunse et al.

Abstract

A large part of the ice discharge from ice caps and ice sheets occurs through spatially limited flow units that may operate in a mode of steady flow or cyclic surge behaviour. Changes in the dynamics of distinct flow units play a key role in the mass balance of Austfonna, the largest ice cap on Svalbard. The recent net mass loss of Austfonna was dominated by calving from marine terminating outlet glaciers. Previous ice-surface velocity maps of the ice cap were derived by satellite radar interferometry (InSAR) and rely on data acquired in the mid-1990s with limited information concerning the temporal variability. Here, we present continuous Global Positioning System (GPS) observations along the central flowlines of two fast flowing outlet glaciers over 2008–2010. The data show prominent summer speed-ups with ice-surface velocities as high as 240 % of the pre-summer mean. Acceleration follows the onset of the summer melt period, indicating enhanced basal motion due to input of surface meltwater into the subglacial drainage system. In 2008, multiple velocity peaks coincide with successive melt periods. In 2009, the principle melt was of higher amplitude than in 2008. Flow velocities appear unaffected by subsequent melt periods, suggesting a transition towards a hydraulically more efficient drainage system. The observed annual mean velocities of Duvebreen and Basin-3 exceed those from the mid-1990s by factors two and four, respectively, implying increased ice discharge at the calving front. Measured summer velocities up to $2\,\mathrm{m\,d^{-1}}$ for Basin-3 are close to that of Kronebreen, often referred to as the fastest glacier on Svalbard.

1 Introduction

Spatially limited flow units are a typical feature of large ice caps and ice sheets and responsible for most of the ice flux from the interior/accumulation area towards the margin/ablation area. Changes in the dynamics of these flow units have strong implications on glacier mass balance. Transported towards the margin, the ice is exposed to

increased surface melt and, in case of marine-terminating outlets, iceberg calving. The calving rate depends on the ice flux towards the calving front and the position change of the terminus. Iceberg calving allows for more rapid and abrupt ice mass loss than surface melt. Its potential contribution to eustatic sea-level rise (SLR) is suggested to account for up to 2 m by the end of this century (Pfeffer et al., 2008). Yet, this contribution is excluded from the last consensus estimate, 0.18 – 0.6 m SLR until 2100, by the Intergovernmental Panel on Climate Change (IPCC) Fourth Assessment (Solomon et al., 2007).

Fast glacier flow is achieved by basal motion rather than by internal deformation and requires basal temperatures at or near the pressure-melting point. Basal motion refers to sliding of the ice base over bedrock (Clarke, 1987) or deformation of subglacial sediments (Clarke et al., 1984; Tulaczyk et al., 2000; Fischer and Clarke, 2001). On shorter timescales (hourly to seasonal), flow variations appear closely linked to changes in effective pressure at the glacier base, i.e. ice overburden reduced by basal water pressure (Meier and Post, 1987). In addition, calving events (Thomas, 2004) or buoyancy perturbations due to ocean tides (O'Neel et al., 2003) may influence the stability of marine termini, and cause velocity fluctuations to propagate up-glacier by means of longitudinal stress coupling (Price et al., 2008; Nick et al., 2009).

Excessive charge of the subglacial drainage system early in the summer melt season increases the basal water pressure, thereby weakening the ice-bed coupling and promoting high velocities in excess of those during winter (Iken and Bindschadler, 1986). While the phenomenon was first observed and studied on temperate alpine glaciers, enhanced ice-surface velocities following surface melt were also reported for the Greenland ice sheet (Zwally et al., 2002) and Arctic glaciers with polythermal regimes (Copland et al., 2003; Rippin et al., 2005; Nuttall and Hodgkins, 2005). In polar environments, glacier acceleration usually lags the onset of summer melt. Meltwater refreezes in the snowpack until the cold-content of the snow (and firn) is diminished and basal lubrication does not occur, before a connection between the supraglacial and englacial/subglacial drainage system is established (Copland et al., 2003). Abrupt

Title Page

Abstract | Introduction

Conclusions | References

Tables | Figures

◄◄ | ►►

◄ | ►

Back | Close

Full Screen / Esc

Printer-friendly Version

Interactive Discussion

and vigorous water input may follow drainage events of supraglacial lakes, that are known to form at the surface of many Arctic glaciers during summer. The relationship between surface melt and glacier acceleration is not linear, but depends on the nature of the basal hydraulic system and the response time needed to adjust for changes in water input. Sustained input of large volumes of meltwater may hamper rather than enhance glacier motion, as recently observed in SW Greenland (van de Wal et al., 2008; Sundal et al., 2011). Model results illustrate that a transition from a hydraulically inefficient distributed drainage system to an efficient channelized system can explain glacier slow-down during sustained melt periods (Schoof, 2010).

Ice-surface velocity maps of good spatial resolution can be determined by satellite radar interferometry (InSAR; e.g. Rott, 2009) or speckle/intensity tracking of SAR intensity images (Strozzi et al., 2002). A disadvantage of these methods is that suitable data is only available for limited time periods. Continuous or repeated ground-based Global Positioning System (GPS) observations yield displacement rates of specific surface points. GPS measurements provide velocity time series at the desired temporal resolution and at high accuracy, however, with limited information on the spatial variability.

At Austfonna, the largest ice cap on Svalbard, InSAR revealed distinct fast-flow units embedded in a slow moving bulk of the ice cap (Dowdeswell et al., 1999; Bevan et al., 2007). These studies rely on data acquired during the winter months of the mid 1990s. They do not capture the seasonal variability and may not reflect the present dynamics of individual outlet glaciers. The ice cap comprises several surge-type basins and its current net mass loss is mainly attributed to calving from the marine ice margin (Dowdeswell et al., 2008; Moholdt et al., 2010). Also the calving estimate of $2.5 \pm 0.5\,\mathrm{km}^3\,\mathrm{a}^{-1}$ w.e. published by Dowdeswell et al. (2008) rely on mid 1990s surface-velocity snapshots.

In this study, we present continuous GPS-measurements along the central flowlines of Duvebreen and Basin-3, two of Austfonna's fast-flow units. The presented GPS records span a two-year period, and allow investigation of seasonal and year-to-year

Seasonal speed-up of two outlet glaciers of Austfonna

T. Dunse et al.

changes in flow velocities. Basin-3 was reported to have undergone a short-lived flow-instability or "mini-surge" in the early 1990s (Dowdeswell et al., 1999). In parallel to the GPS data, we consider the temperature record of a nearby automatic weather station (AWS) to investigate a possible relationship between surface melt and flow dynamics and compare the recently measured flow velocities with those from the mid 1990s.

2 Survey area

2.1 The Austfonna ice cap

Austfonna is a ~8000 km^2 large ice cap centered at 79.7° N, 24.0° E on the island Nordaustlandet, in the northeast of Svalbard (Fig. 1).

The ice cap represents the largest ice body on the highly glacierized archipelago. It consists of one main dome that rises to 800 m a.s.l., where the ice thickness reaches its maximum of about 580 m (Dowdeswell et al., 1986). A main ice divide separates the northwestern basins, predominantly terminating on land or in narrow fjords, from the southeastern basins, that are to a large extent grounded below sea level and form an almost continuous calving front towards the Barents Sea (Dowdeswell, 1986; Hagen et al., 1993). The general ice-surface velocity pattern derived from InSAR data acquired in January 1994 is typical for a slow moving Arctic ice cap. The bulk of the ice is moving at low velocities < 10 m a^{-1}, interrupted by spatially limited flow units characterized by enhanced ice surface velocities in the range of about 50–250 m a^{-1} and coincident with subglacial valleys or troughs (Dowdeswell et al., 1999). Model results suggest that the large ice thickness within these valleys allows for temperate basal conditions, and hence, basal motion as the dominant mechanism of ice flow (Dunse et al., 2011). Several basins are known to have surged in the past, specifically Etonbreen and Bråsvellbreen in the 1930s and Basin-3 between 1850-70 (Schytt, 1969; Lefauconnier and Hagen, 1991). A submarine push-moraine in front of Basin-5, a northeastern neighbour of Basin-3, suggests that also this basin may have surged, probably within

the past 100 years (Robinson and Dowdeswell, 2011). Currently observed elevation changes with interior thickening at rates of up to 0.5 m a^{-1} and marginal thinning at 1–3 m a^{-1} (Bamber et al., 2004; Moholdt et al., 2010) can be explained by low ice flux rates within surge-type basins in their quiescent phase (Hagen et al., 2005; Bevan et al., 2007). Geodetically derived mass balance for the time period 2002–08 suggest a surface mass balance close to zero with a mean equilibrium-line altitude (ELA) of about 450 m a.s.l. for the northwestern and 300 m a.s.l. for the southeastern basins. For 2008, mass balance stakes indicate an unusual low ELA (Moholdt et al., 2010). Yet, the net mass balance of Austfonna is negative, -1.3 ± 0.5 km^3 a^{-1}, due to calving and retreat of the marine ice margin at rates of several tens of meters per year during the past few decades (Dowdeswell et al., 2008).

Here, we focus on the central flowlines of two fast-flowing outlet glaciers along which surface velocities have been determined earlier by Dowdeswell et al. (1999): Duvebreen in the northwestern and Basin-3 in the southeastern section of the ice cap (Fig. 1). When the flowlines were visited on 25 August 2008, a continuous winter snow cover persisted down to the calving termini. In 2009 the ELA was positioned higher up than in 2008, but still below average, at about 200 m a.s.l. on both Duvebreen and Basin-3. In the following, we present general features of the dynamics of the two basins and the geometry along their central flowline. The latter is based on ground-penetrating radar and kinematic GPS data, further described in Sect. 3.2 and Appendix A. Each flowline is defined by five specific survey locations, equidistantly distributed over a length of 16 km (Fig. 2).

2.2 Basin-3

Basin-3 coincides with the eastern half of a major valley that runs west-eastwards across Nordaustlandet. A large area of the basin is marine grounded down to depths of ~150 m below sea level and the terminus calves into the Barents Sea (Dowdeswell, 1986). Basin-3 has surged some years prior to 1873 (Lefauconnier and Hagen, 1991). The terminus has retreated ~8 km from its maximum extent marked by the position of

a large submarine push moraine since (Robinson and Dowdeswell, 2011). The observed surface profile is relatively flat (Dowdeswell, 1986). This may be indicative for the early quiescent phase (Meier and Post, 1969), thus implying a long, multi-century surge cycle. Alternatively, the flat surface profile could be explained by a considerable contribution of basal motion to the overall ice flow. Along the surveyed section of the flowline, surface elevations rise from 121 m a.s.l., ~5 km from the calving front, to 356 m a.s.l. with a mean surface slope of 0.84° (Fig. 2 a). The glacier is grounded below sea level along the entire section. The bedrock is relatively flat over the lower 12 km, with bedrock elevations around −100 m a.s.l. Further upstream, the bedrock rises to near sea level and features two bedrock protrusions. The ice thickness gradually thickens upglacier from 220 to 361 m and a mean of 313 m.

InSAR analysis based on SAR scenes acquired in the early 1990s revealed a distinct flow unit of 5–6 km width, topographically constrained by Isdomen, a prominent subglacial hill to the north (Dowdeswell et al., 1999). Velocities in February 1992 were as high as 140 m a^{-1} at the terminus, whereas in January 1994, only 80 m a^{-1} were observed. Visible Landsat imagery suggest that the flow unit was fairly inactive between 1973–91 and that fast flow was initiated after 1991. Calculated balance velocities were one order of magnitude smaller than the observed surface velocities. Dowdeswell et al. (1999) thus interpreted the change in flow velocities as a short-lived flow instability or mini-surge initiated after 1991, arguing that the ice flux cannot be sustained under the present climate.

2.3 Duvebreen

Duvebreen, in the northwest of Austfonna, drains into the narrow Duvefjorden where the terminus forms a ~2 km wide calving front towering ~30 m above the water surface. InSAR-derived velocities for February 1992 and January 1994 ranged from 20–80 m a^{-1} along the central flowline (Dowdeswell et al., 1999).

Surface elevations along the surveyed section range from 207 m a.s.l., 4–5 km upglacier from the calving front, to 548 m a.s.l. with a mean surface slope of 1.22°

(Fig. 2 b). The ice thickness ranges from ~300 m at the lower to >400 m at the upper end, with a mean of 328 m. The bedrock topography is relatively flat in the upper half, with elevations ranging from 100–160 m a.s.l. Further downglacier, the bedrock abruptly drops down to sea level and beyond, reaching depths of more than 100 m below sea level. Bedrock protrusions of several 100 m in diameter and 20–30 m heights promote local increase in ice-bed coupling and hence, compressive flow. Convex ice-surface undulations therefore appear slightly upglacier from bedrock protrusions. Vice-versa, concave surface elevations coincide with downglacier sloping bedrock. A very prominent surface depression lies upglacier from the bedrock escarpment. Field inspections in spring 2008 suggest that a supra-glacial lake may form within the depression during the summer melt season.

3 Methods

In spring 2008, we established a series of stakes along the central flowlines of Duvebreen and Basin-3. Each flowline was surveyed by five GPS recording units, mounted atop the stakes, drilled in the glacier ice at 4 km intervals, numbered ♯1 – 5 in upglacier direction (Fig. 2; Table 1). Maintenance and data retrieval took place in early May 2009 and 2010 during the annual ground-based field season and during a short visit in August 2009. The lower units were positioned in highly crevassed areas with a thin snow cover in May 2009, and hence weak snow bridges, prohibiting access of all units on Basin-3 (B3 ♯1–5) and the lowermost one on Duvebreen (Duve ♯1). Insufficient power-supply caused a gap in the observations between June and August 2009.

3.1 Continuous Global Positioning System (GPS) observations

We utilized single-frequency GPS receivers that operate unmaintained over time periods of 1 year or longer (van de Wal et al., 2008; den Ouden et al., 2010). The receivers switch on every hour for a period of 3 min to allow the system to stabilize. Subsequently, positions are computed within the receiver and the geographical position and time are

logged. Post-processing capabilities are restricted by the limited information stored, i.e. we do not apply correction with respect to atmospheric effects such as ionospheric and tropospheric delay, clock information or satellite configuration. Instead, the simple broadcast orbits with the WGS84 reference frame are used and a running average is applied to remove high frequency noise at the cost of temporal resolution. Based on the standard deviation of the average position of a reference station in central Spitsbergen during 2006 – 2009, the horizontal accuracy of the system was determined to be 1.62 m (den Ouden et al., 2010). Our measurement period largely overlaps with the period investigated by den Ouden et al. (2010) and is characterized by a solar ionospheric minimum. A greater error associated with the neglected ionospheric delay and hence, uncertainty in the positioning is to be expected in years with higher solar activity.

The raw data consists of hourly records of the geographical position and the associated date and time. Outliers and data gaps are identified by determining the standard deviations within a moving time window of 72 hours. An individual dataset entry is disregarded, if it raises the standard deviation of either the latitude or longitude above a specified threshold (e.g. 10 %). Outliers and data gaps may result from loss of energy supply, bad satellite reception, e.g. due to riming of the antennas or external disturbances of the satellite signal, such as ionospheric effects. Daily displacements in the range of 0.1 – 1 m are within the uncertainty of the system's position measurements. Thus, data averaging over multiple days is required to yield meaningful results. The cleaned raw data is converted to UTM33X and a daily mean position (at hour 1200) is assigned, if at least 12 out of 24 samples of a particular day are available. The daily averages are characterized by significant noise reduction, compared to the hourly raw data (Fig. 3a). A 7 day running mean is applied independently to the daily Easting and Northing. This further enhances the robustness of the position measurement, however, at the cost of the temporal resolution. Daily displacements and hence velocities are calculated from the averaged positions utilizing the theorem of Pythagoras. Considering the small horizontal scales discussed here, the curvature of the Earth can be neglected. Finally, the velocity record is smoothed by applying a second 7-day

running-mean (Fig. 3b). Daily averaging has been shown to reduce the standard deviation in the position measurement to <0.5 m (den Ouden et al., 2010). Accordingly, the maximum error in the displacement between consecutive days is $1\,\mathrm{m\,d^{-1}}$ ($365\,\mathrm{m\,a^{-1}}$). The error in displacement between two arbitrary daily mean positions, e.g. at the beginning and end of a 1 year period, remains unaffected and the accuracy increases significantly, i.e. to $1\,\mathrm{m\,a^{-1}}$. Annual velocities according to the mean of the computed daily velocities differ from annual velocities inferred by the begin-end method by typically less than 1%. Exceptions can be explained with incomplete records of daily values within a certain period. This indicates that the filtering of the GPS data provides robust estimates of ice-surface velocities.

3.2 Additional data

Low-frequency ground-penetrating radar (GPR) and ground-based kinematic Global Navigation Satellite System (GNSS; GPS and GLONASS) observations were collected in spring 2008 and combined to derive glacier geometry along the flowlines. Where GPR measurements are lacking, bedrock elevations are interpolated utilizing additional information from a bedrock map at 1 km horizontal resolution (Dunse et al., 2011). A detailed description of the methodology is provided in Appendix A.

The air temperature record from an AWS, located in the western part of Austfonna at 510 m a.s.l., (Fig. 1; Schuler et al., 2007) is used to derive time series of cumulative positive degree-days (PDD) over the summer months. The annual PDD is the sum of daily mean air temperatures above melting over the period of an entire melt season (counted in °C d) and an indicator for surface melt (Reeh, 1989). The temperature record is not modified to account for the specific location or surface elevation of individual stakes, e.g. by application of a temperature lapse rate. Doing so, would result primarily in a shift in the absolute PDD values, but would not affect the timing of significant melt periods. In summer 2008, the PDD reached 52 °C d, with maximum diurnal temperatures up to ~2.5 °C, while throughout summer 2009, the PDD was significantly larger, 78 °C d and maximum temperatures reached ~3.5 °C.

4 Results

4.1 Ice-surface velocities: 2008/2009 vs. 2009/2010

The GPS records span the time period from May 2008 to May 2010 and allow investigation of seasonal and interannual changes in ice-surface velocities. Over the measurement period , ice-surface velocities decreased with distance upglacier along the central flowlines (Fig. 4). In 2008, a prominent summer speed-up occurred at all stations on Basin-3 (Fig. 4 a). Subsequently, ice-surface velocities gradually decreased from their summer maxima maintaining relatively high speeds during the winter months compared to the pre-summer minimum, occurring in June. Velocities in June 2009 were above those observed in June 2008. Unfortunately, the summer speed-up of Basin-3 was not captured in 2009, but measured velocities from late summer 2009 until May 2010 appear to be shifted to higher values, compared to the corresponding period of the previous year. Annual mean velocities during May 2008 to May 2009 ranged from ca. $120\,\mathrm{m\,a^{-1}}$ at B3 #5 to $400\,\mathrm{m\,a^{-1}}$ at B3 #1 (Table 2). Over the period May 2009–2010, velocities increased by 21–41%.

At Duvebreen, ice-surface velocities maintained a steady level over the two-year period, with short-lived summer speed-ups noticeable at the lower locations (Fig. 4b). Within a few weeks after the summer maximum, velocities returned to pre-summer values. Annual mean velocities ranged from $40\,\mathrm{m\,a^{-1}}$ at Duve #5 to $200\,\mathrm{m\,a^{-1}}$ at Duve #1. In 2009/2010, the annual mean velocity decreased by ca. 10% at the lowermost stake (Duve #1), compared to 2008/2009, while velocities at the other measured locations (Duve #2–4) did not change significantly. The GPS unit at Duve #5 did not function in 2009/2010.

4.2 Summer speed-up 2008 and 2009

Ice-surface velocities at Basin-3 underwent a clear annual cycle with lowest velocities preceding a prominent summer speed-up (Fig. 4). During June, the velocities were

characterized by a quasi-stationary pre-summer low. The associated monthly means and standard deviations provide a reference against which to compare maximum summer velocities. We define the onset of the summer speed-up at a particular location as the day where velocities are in excess of three standard deviations from the pre-summer mean. The summer speed-up was initiated at the lowest location and occured with several days delay between stations located further upglacier (Figs. 5 and 6). The summer maximum, however, was reached at about the same day at all locations of a particular flowline (Table 3). At Basin-3, in summer 2008, a summer speed-up was detected at all locations with a onset-delay of 11 days at the highest location (B3 #5) compared to the lowermost (B3 #1; Fig. 5a). The maximum summer velocity was reached 9–25 days after the onset date, in the beginning of August (29 July–3 August) and ranged from $143.2\,\mathrm{m\,a^{-1}}$ to $698.5\,\mathrm{m\,a^{-1}}$. This corresponds to a velocity increase of 53–140 % compared to the pre-summer mean. The relative acceleration is smallest at the uppermost station and increases further downglacier. At Duvebreen, the summer speed-up was less pronounced and only noticeable at the locations further downglacier along the flowline (Fig. 5b).

The 2008 summer speed-up was characterized by 3 distinct peaks, concurrent at all locations. The second and third peaks followed ~2 and 7 weeks after the primary summer maxima. (Fig. 5a, b). The initial summer speed-up coincided with the first prolonged period with air temperatures above 0 °C in the second half of July (Fig. 5c). The two other velocity peaks coincided with a second and third period of melting that lead to a significant rise in cumulative PDD. In 2009, summer velocities were only recorded at 3 locations of Duvebreen (Duve #2–4; Fig. 6). The 2009 summer speed-up at these locations was of higher amplitude (Table 3) and also detected further upglacier than in 2008, where only the two lowermost stakes (Duve #1–2) showed significant acceleration.

5 Discussion

5.1 Surface-velocities fluctuations

The distinct characteristics of the summer-speed up in 2008 and 2009 can be explained by the total volume of surface-generated meltwater and the timing of the input into the subglacial drainage system. Summer 2008 was characterized by relatively low air temperatures, yielding a low cumulative PDD and hence, little surface melt. Snow cover persisted over the ice cap throughout the entire summer season and is likely to have maintained high surface albedo, thereby reducing the energy available for melt. The input of small volumes of melt water to the subglacial system may not have been sufficient to establish an efficient drainage system. Consequently, renewed melt water input during late-summer melt periods, associated with a distinct increase in cumulative PDD, presumably provoke high subglacial water pressure and enhanced hydraulic lubrication. In 2009, air temperatures were significantly higher, yielding a cumulative PDD of 78 °C d, compared to only 52 °C d in 2008. The summer speed-up in 2009 coincided with a strong increase in cumulative PDD. A second significant melt period in the end of August had no clear effect on the observed surface motion, in contrast to comparable melt periods in 2008. This indicates that in 2009, the basal drainage system was able to accommodate the increased input of meltwater likely associated with the warm events, without weakening the ice-bed coupling. This in turn implies that a hydraulically efficient drainage system evolved earlier in summer during the principle melt period (late July to early August). At both flowlines, an upglacier propagation of the onset of the summer speed-up was observed. This can be explained by a later onset of surface melt and hence local input of meltwater into the englacial/subglacial drainage system, together with longitudinal coupling, with increased delay in the response of upglacier ice regions to a speed-up initiated further downglacier.

At Basin-3, the decrease from the summer-2008 velocity peak was slow and gradual. This indicates that also basal water pressure remained at a high level and only decreased gradually. An inefficient drainage system may have retained a significant

Seasonal speed-up of two outlet glaciers of Austfonna

T. Dunse et al.

fraction of basal water throughout the winter months, thereby facilitating continuous, though diminishing basal lubrication or plastic deformation of water-saturated sediments. The bedrock slope along the surveyed profile is gentle and lies below sea level along its entire length, providing little topographic resistance to basal sliding and facilitating upglacier propagation of velocity fluctuations through longitudinal coupling. This may explain why the summer speed-up is noticeable at all locations, albeit at decreasing amplitude further upglacier. The observed acceleration of Basin-3 in 2009/2010 compared to 2008/2009 could be explained by a general shift of the basal water pressure towards higher values, but this remains speculative, as no information of basal hydrology is available.

At Duvebreen, the multiple summer speed-ups in 2008 and the single one in 2009 were short-lived in nature. The surface velocity quickly returned to pre-summer values. This may be explained by a rapid transition from a hydraulically inefficient, distributed drainage system to a hydraulically efficient, channelized system. Another explanation is provided by the specific topography, which is fundamentally different than that of Basin-3. At the uppermost 3 stakes on Duvebreen (Duve #3–5) the glacier is grounded about 100 m a.s.l. (Fig. 2). Duve #2 is located just downglacier of a steep drop into the narrow Duvefjord, where bedrock elevations reach deeper than −100 m a.s.l. (Duve #1). The steep valley walls may possess significant lateral drag upon the lower section of the glacier, i.e. below Duve #2. Additional basal lubrication has to compensate for the lateral drag. This may only be fulfilled in periods where the basal water pressure exceeds a certain threshold. Lateral shear may thus stabilize the terminus of Duvebreen and make the glacier less prone to terminus fluctuations and/or longitudinal coupling of changes in terminus dynamics, initiated at the calving front. The steep bedrock topography at Duve #2 promotes the formation of surface crevasses (those have also been observed in the field) and facilitates meltwater routing to the bed. The presence of soft sediments and a reduction in effective normal pressure may alternatively explain the sensitivity of the marine grounded section to flow perturbations as also suggested by recent model experiments (Dunse et al., 2011). In 2009, surface melt and input of

meltwater into the englacial/subglacial drainage system may have occurred at higher elevation, causing noticeable summer speed-up also at higher stations.

5.2 Implications for iceberg calving

Changes in the dynamics of marine terminating glaciers have a direct impact on the iceberg discharge. The calving flux, q_c, is determined by the ice flux through the calving front and the position change of the front. Following van der Veen (1996) the calving flux can be expressed as:

$$q_c = (\overline{u}_c - \frac{dL}{dt}) \cdot hw \tag{1}$$

where $\overline{u}_c$ is the depth-averaged velocity at the calving front, $\frac{dL}{dt}$ the change in front position over time (positive in case of advance, negative in case of retreat) and h and w are the vertical and horizontal dimensions of the calving front.

Using the InSAR-derived surface velocities, Dowdeswell et al. (1999) investigated the ice flux within the flow unit of Basin-3 . Estimating the cross-sectional area to 5 km × 240 m, ~7.5 km upglacier from the marine ice margin, and assuming a depth-averaged velocity corresponding to 85 % of the measured surface velocity, 90 m a^{-1} in winter 1992 and 50 m a^{-1} in winter 1994, the ice flux amounted to 0.1 and 0.05 km^3 a^{-1} respectively. Dowdeswell et al. (2008) provided a total calving estimate for Austfonna, distinguishing between the ice-flux through the calving front and margin-change flux contribution of individual basins. The calving flux from Basin-3 was dominated by marginal retreat, accounting for 0.3 km^3 a^{-1} out of a total 0.45 km^3 a^{-1}. The ice flux through the calving front contributed 0.15 km^3 a^{-1}. The calving flux from Duvebreen was dominated by the ice-flux contribution, accounting for ~75 % of a total calving flux of 0.1 km^3 a^{-1}.

Dowdeswell et al. (1999, 2008) considered his annual ice flux estimates to represent a lower limit, because flow rates during the winter months December to February, corresponding to the acquisition period of the SAR data used, are usually lower than

Title Page

Abstract | Introduction

Conclusions | References

Tables | Figures

|◄ | ►|

◄ | ►

Back | Close

Full Screen / Esc

Printer-friendly Version

Interactive Discussion

average. However, our two-year record indicate that velocities in December to February are approximately equal or, in case of Basin-3 over the period 2009–2010, even slightly larger than the corresponding annual average (Fig. 4). Mean-annual velocities 2009/2010 of 479 m a^{-1} at B3 #1 and 444 m a^{-1} at B3 #2 (Table 2), about 4–5 km and 8–9 km from the marine margin, indicate a more than four-fold velocity increase compared to those used to derive previous ice flux estimates. Applied to the flux-gate defined by Dowdeswell et al. (1999), the ice flux within Basin-3 increased from 0.1 km^3 a^{-1} in 1992 to 0.45 km^3 a^{-1} in 2009/2010, indicating that the ice flux contribution may have surpassed the contribution from marginal retreat. The flow velocities along the central flowline of Duvebreen doubled from 20–80 m a^{-1} in the mid-1990's to 35–200 m a^{-1} in 2008–2010, also suggesting an increased ice-flux contribution to the total calving flux. New data on the marine outline is required to assess the total calving flux.

6 Conclusions

Annual mean and mean winter flow velocities of Duvebreen over the period 2008–2010 were twice as high as those inferred for winter in the 1990s. The spatial velocity pattern and the characteristics of summer speed-up appear to be controlled by the distinct topography with the lower part of the glacier flowing over an escarpment and being channelled into a deep and narrow fjord. Likewise, Basin-3 has accelerated by about a factor four compared to the 1990s and showed also an acceleration of 30–40 % from 2008/2009 to 2009/2010. Velocities measured during summer 2008 reach up to 2 m d^{-1} (700 m a^{-1}) within 5 km from the calving front and are as high as those reported from Kronebreen, often referred to as the fastest tidewater glacier on Svalbard, with annual mean velocities up to 1.5 m d^{-1}/550 m a^{-1} (Lefauconnier et al., 1994) and recent summer maxima of 2.5 m d^{-1} measured at the calving front (Rolstad et al., 2009).

In 2008, the observed summer speed-up of both Basin-3 and Duvebreen appears closely linked to positive diurnal air temperatures/cumulative PDD, a proxy for surface

Full Screen / Esc

Printer-friendly Version

Interactive Discussion

melt and potential input of meltwater into the englacial/subglacial drainage system. In 2009, GPS observations only cover the speed-up of Duvebreen. Summer 2009 was significantly warmer than summer 2008 with a pronounced principle melt period (late July to early August) and the relationship between ice-surface velocity and air temperature is more complex. Meltwater volumes produced later in the melt season do not lead to positive excursions in glacier flow. This indicates that a hydraulically effective drainage system has established in the course of the principle melt period and increased meltwater input can therefore be accommodated without raising basal water pressure and enhancing basal lubrication.

Appendix A

Derivation of glacier geometry along flowlines

To derive the glacier geometry along the flowlines, we combine surface elevation profiles from ground-based kinematic GNSS with low-frequency GPR measurements of ice thickness. Kinematic GNSS observations were logged at a rate of 1 Hz (approx. every 5.5 m) and differentially post-processed using a stationary GNSS as reference, yielding an accuracy of typically better than 5 cm in horizontal position and 10 cm in height (Eiken et al., 1997). GPR (VIRL-6) measurements were triggered every 2 m by means of an odometer. Navigation data was recorded simultaneously with the GPR data using a GPS Garmin II Plus receiver (Vasilenko et al., 2010). The radar transmitter generates pulses of 25 ns duration with a center frequency of 20 MHz, resulting in a system resolution of approximately 2 m (assuming a radio-wave velocity of $0.168 \pm 0.0005 \, \mathrm{m \, ns^{-1}}$, typical for cold ice). The precision of the ice thickness measurements was estimated to ~1.6 m, based on the standard deviation in ice thickness at more than 34000 crossover points from the entire Austfonna survey (personal communication G. Moholt, Department of Geosciences, University of Oslo, Oslo, Norway, 2011). The precision represents the error in ice thickness due to the uncertainty in

the time measurement (digitization of bedrock reflection). The accuracy in ice thickness is determined when adding an absolute error of about 0.3 % (3 mm per meter ice) to the precision value. This absolute error is related to the uncertainty of radio-wave velocity. For an ice thickness of 350 m this corresponds to an error of about 1 m ($2000\,\text{ns} \times 0.0005\,\text{m\,ns}^{-1}$) yielding an accuracy of the GPR-derived ice thickness of about 2.6 m.

To link kinematic GPS and GPR measurements along the flowline, linear legs between consecutive stake positions have been taken as benchmark distance. A correction factor, specific for each dataset and leg (typically between 0.98 and 1) is then applied to all distance increments so that the cumulative distance along the measured tracks matches the benchmark distance. Both datasets are resampled at 10 m intervals to allow subtraction of ice thickness from surface elevation to derive bedrock elevation. Gaps in the GPR record are padded by extracting values from an ice thickness map at 1 km horizontal resolution (Dunse et al., 2011). Values were extracted for positions corresponding to 1 km intervals along the flowlines and corrected for a mean bias, determined from the overlapping sections (mean and standard deviation of $-16.61 \pm 11.59\,\text{m}$ in the case of Basin-3; $-1.11 \pm 7.80\,\text{m}$ in the case of Duvebreen).

Seasonal speed-up of two outlet glaciers of Austfonna

T. Dunse et al.

Title Page

Abstract	Introduction
Conclusions	References
Tables	Figures

◀◀   ▶▶

◀   ▶

Back   Close

Full Screen / Esc

Printer-friendly Version

Interactive Discussion

References

Bamber, J., Krabill, W., Raper, V., and Dowdeswell, J.: Anamolous recent growth of part of a large Arctic ice cap: Austfonna, Svalbard, Geophys. Res. Lett., 31, L12402, doi:10.1029/2004GL019667, 2004. 3428

5 Bevan, S., Luckman, A., and Murray, T.: Positive mass balance during the late 20th century on Austfonna, Svalbard revealed using satellite interferometry, Ann. Glaciol., 46, 117–122, 2007. 3426, 3428

Clarke, G.: Fast glacier flow - ice streams, surging, and tidewater glaciers, J. Geophys. Res.-Solid, 92, 8835–8841, 1987. 3425

10 Clarke, G., Collins, S., and Thompson, D.: Flow, thermal structure, and subglacial conditions of a surge-type glacier, Can. J. Earth Sci., 21, 232–240, 1984. 3425

Copland, L., Sharp, M. J., and Nienow, P. W.: Links between short-term velocity variations and the subglacial hydrology of a predominantly cold polythermal glacier, J. Glaciol., 49, 337–348, 2003. 3425

15 den Ouden, M. A. G., Reijmer, C. H., Pohjola, V., van de Wal, R. S. W., Oerlemans, J., and Boot, W.: Stand-alone single-frequency GPS ice velocity observations on Nordenskiöldbreen, Svalbard, The Cryosphere, 4, 593–604, doi:10.5194/tc-4-593-2010, 2010. 3430, 3431, 3432

Dowdeswell, J.: Drainage-basin characteristics of Nordaustlandet ice caps, Svalbard, J. Glaciol. , 32, 31–38, 1986. 3427, 3428, 3429

20 Dowdeswell, J., Drewry, D., Cooper, A., Gorman, M., Liestøl, O., and Orheim, O.: Digital mapping of the Nordaustlandet ice caps from airborne geophysical investigations, Ann. Glaciol., 8, 51–58, 1986. 3427

Dowdeswell, J. A., Unwin, B., Nuttall, A. M., and Wingham, D. J.: Velocity structure, flow instability and mass flux on a large Arctic ice cap from satellite radar interferometry, Earth Planet.
25 Sci. Lett., 167, 131–140, 1999. 3426, 3427, 3428, 3429, 3437, 3438

Dowdeswell, J. A., Benham, T. J., Strozzi, T., and Hagen, J. O.: Iceberg calving flux and mass balance of the Austfonna ice cap on Nordaustlandet, Svalbard, J. Geophys. Res.-Earth, 113, F03022, doi:10.1029/2007JF000905, 2008. 3426, 3428, 3437

Dunse, T., Greve, R., Schuler, T. V., and Hagen, J. O.: Permanent fast flow versus cyclic surge
30 behaviour: numerical simulations of the Austfonna ice cap, Svalbard, J. Glaciol. , 57, 247–259, 2011. 3427, 3432, 3436, 3440

Eiken, T., Hagen, J. O., and Melvold, K.: Kinematic GPS survey of geometry changes on

Svalbard glaciers, Ann. Glaciol., 24, 157–163, 1997. 3439

Fischer, U. H. and Clarke, G. K. C.: Review of subglacial hydro-mechanical coupling: Trapridge Glacier, Yukon Territory, Canada, Quaternary International, 86, Int Union Quaternary Assoc, doi:10.1016/S1040-6182(01)00049-0, 2001. 3425

5 Hagen, J., Liestøl, O., Roland, E., and Jørgensen, T.: Glacier Atlas of Svalbard and Jan Mayen, Norsk Polarinstitutt, Oslo, Norway, 1993. 3427

Hagen, J., Eiken, T., Kohler, J., and Melvold, K.: Geometry changes on Svalbard glaciers: mass-balance or dynamic response?, Ann. Glaciol., 42, 255–261, 2005. 3428

Iken, A. and Bindschadler, R. A.: Combined Measurements of Subglacial Water-pressure and
10 Surface Velocity of Findelengletscher, Switzerland – Conclusions About Drainage System and Sliding Mechanism, J. Glaciol., 32, 101–119, 1986. 3425

Lefauconnier, B. and Hagen, J.: Surging and Calving Glaciers in Eastern Svalbard, Norsk Polarinstitutt, Oslo, Norway, 1991. 3427, 3428

Lefauconnier, B., Hagen, J., and Rudant, J.: Flow Speed and Calving Rate of Kongsbreen
15 Glacier, Svalbard, Using Spot Images, Polar Res., 13, 59–65, 1994. 3438

Meier, M. and Post, A.: What are glacier surges, Canadian Journal of Earth Sciences, 6, 807–817, 1969. 3429

Meier, M. and Post, A.: Fast tidewater glaciers, J. Geophys. Res.-Solid, 92, 9051–9058, 1987. 3425

20 Moholdt, G. and Kääb, A.: A new DEM of the Austfonna ice cap by combining differential SAR interferometry with ICESat laser altimetry, Polar Res., in press., 2011. 3448

Moholdt, G., Hagen, J. O., Eiken, T., and Schuler, T. V.: Geometric changes and mass balance of the Austfonna ice cap, Svalbard, The Cryosphere, 4, 21–34, doi:10.5194/tc-4-21-2010, 2010. 3426, 3428

25 Nick, F., Vieli, A., Howat, I., and Joughin, I.: Large-scale changes in Greenland outlet glacier dynamics triggered at the terminus, Nat. Geosci., 2, 110–114, 2009. 3425

Nuttall, A. M. and Hodgkins, R.: Temporal variations in flow velocity at Finsterwalderbreen, a Svalbard surge-type glacier, Ann. Glaciol., 42, 71–76, 2005. 3425

O'Neel, S., Echelmeyer, K. A., and Motyka, R.: Short-term variations in calving of a tidewater
30 glacier: LeConte Glacier, Alaska, USA, J. Glaciol., 49, 587–598, 2003. 3425

Pfeffer, W. T., Harper, J. T., and O'Neel, S.: Kinematic constraints on glacier contributions to 21st-century sea-level rise, Science, 321, 1340–1343, 2008. 3425

Price, S. F., Payne, A. J., Catania, G. A., and Neumann, T. A.: Seasonal acceleration of inland

Seasonal speed-up of two outlet glaciers of Austfonna

T. Dunse et al.

ice via longitudinal coupling to marginal ice, J. Glaciol., 54, 213–219, 2008. 3425

Reeh, N.: Parameterization of melt rate and surface temperature on the Greenland ice sheet, Polarforschung, 59, 113–128, 1989. 3432

Rippin, D. M., Willis, I. C., Arnold, N. S., Hodson, A. J., and Brinkhaus, M.: Spatial and temporal variations in surface velocity and basal drag across the tongue of the polythermal glacier midre Lovenbreen, Svalbard, J. Glaciol., 51, 588–600, 2005. 3425

Robinson, P. and Dowdeswell, J.: Submarine landforms and the behavior of a surging ice cap since the last glacial maximum: The open-marine setting of eastern Austfonna, Svalbard, Mar. Geol., 286, 82–94, doi:10.1016/j.margeo.2011.06.004, 2011. 3428, 3429

Rolstad, C., Chapuis, A., and Norland, R.: Electromagnetic interference in ground-based interferometric radar data from Kronebreen (Svalbard) calving front due to multipath scattering and tidal cycles, J. Glaciol., 55, 943–945, 2009. 3438

Rott, H.: Advances in interferometric synthetic aperture radar (InSAR) in earth system science, Prog. Phys. Geog., 33, 769–791, 2009. 3426

Schoof, C.: Ice-sheet acceleration driven by melt supply variability, Nature, 468, 803–806, 2010. 3426

Schuler, T., Loe, E., Taurisano, A., Eiken, T., Hagen, J., and Kohler, J.: Calibrating a surface mass-balance model for Austfonna ice cap, Svalbard, Ann. Glaciol., 46, 241–248, 2007. 3432

Schytt, V.: Some comments on glacier surges in eastern Svalbard, Can. J. Earth Sci., 6, 867–871, 1969. 3427

Solomon, S., Qin, D., Manning, M., Chen, Z., Marquis, M., Averyt, K., Tignor, M., and Miller, H. L. (eds.): Climate Change 2007: The Physical Science Basis. Contribution of Working Group I to the Fourth Assessment Report of the Intergovernmental Panel on Climate Change, Cambridge University Press, Cambridge, United Kingdom and New York, NY, USA, http://www.worldcat.org/isbn/0521705967, 2007. 3425

Strozzi, T., Luckman, A., Murray, T., Wegmüller, U., and Werner, C. L.: Glacier motion estimation using SAR offset-tracking procedures, IEEE T. Geosci. Remote, 40, 2384–2391, 2002. 3426

Sundal, A. V., Shepherd, A., Nienow, P., Hanna, E., Palmer, S., and Huybrechts, P.: Melt-induced speed-up of Greenland ice sheet offset by efficient subglacial drainage, Nature, 469, 521–524, http://www.nature.com/nature/journal/v469/n7331/full/nature09, 2011. 3426

Thomas, R. H.: Force-perturbation analysis of recent thinning and acceleration of Jakobshavn

Title Page

Abstract | Introduction

Conclusions | References

Tables | Figures

|◀ | ▶|

◀ | ▶

Back | Close

Full Screen / Esc

Printer-friendly Version

Interactive Discussion

Isbræ, Greenland, J. Glaciol. , 50, 57–66, 2004. 3425

Tulaczyk, S., Kamb, W. B., and Engelhardt, H. F.: Basal mechanics of Ice Stream B, West Antarctica 1. Till mechanics, J. Geophys. Res.-Solid, 105, 463–481, 2000. 3425

van de Wal, R. S. W., Boot, W., van den Broeke, M. R., Smeets, C. J. P. P., Reijmer, C. H.,
Donker, J. J. A., and Oerlemans, J.: Large and rapid melt-induced velocity changes in the ablation zone of the Greenland Ice Sheet, Science, 321, 111–113, 2008. 3426, 3430

van der Veen, C.: Tidewater calving, J. Glaciol., 42, 375–385, 1996. 3437

Vasilenko, E., Navarro, F., Dunse, T., Eiken, T., and Hagen, J.: New low-frequency radio-echo soundings of Austfonna ice cap, Svalbard, in: The Dynamics and Mass Budget of Arctic
Glaciers. Extended abstracts, Workshop and GLACIODYN (IPY) meeting, 16–19 February 2009, Kananaskis, Canada., edited by Ahlstrøm, A. and Sharp, M., vol. 127 of *Danmarks og Grønlands geologiske undersøkelse rapport*, GEUS, Copenhagen: IASC Working Group on Arctic Glaciology, 2010. 3439

Zwally, H. J., Abdalati, W., Herring, T., Larson, K., Saba, J., and Steffen, K.: Surface melt-
induced acceleration of Greenland ice-sheet flow, Science, 297, 218–222, 2002. 3425

Title Page

Abstract | Introduction

Conclusions | References

Tables | Figures

◀ | ▶

◀ | ▶

Back | Close

Full Screen / Esc

Printer-friendly Version

Interactive Discussion

Table 1. Survey locations of stakes along the central flowlines of Basin-3 (B3 #1–5) and Duve-breen (Duve #1–5) and their glacier-geometric characteristics. Positions are measured directly and the associated absolute error given in the last row is constant. Ice thickness and hence, bedrock elevation are indirectly measured, the associated error is ice-thickness depended.

Stake (no.)	Latitude (decim. ° N)	Longitude (decim. ° E)	Surface alt. (m a.s.l.)	Ice thickness (m a.s.l.)	Bedrock elev. (m)
B3 #1	79.4992370	25.468043	121.18	219.99 ± 13.84*	−98.81 ± 13.94*
B3 #2	79.4976114	25.273292	184.21	280.78 ± 14.03*	−96.57 ± 14.13*
B3 #3	79.5032166	25.077680	249.41	328.95 ± 2.58	−79.54 ± 2.68
B3 #4	79.5136708	24.889501	282.38	357.10 ± 2.66	−74.72 ± 2.76
B3 #5	79.5279278	24.710116	355.86	360.94 ± 14.26*	−5.08 ± 14.36*
Duve #1	80.1421759	23.958117	207.15	309.00 ± 2.52	−101.854 ± 2.62
Duve #2	80.1117554	24.063358	308.36	301.67 ± 2.50	6.685 ± 2.60
Duve #3	80.0760756	24.047865	391.36	299.82 ± 2.49	91.541 ± 2.59
Duve #4	80.0406765	24.007224	482.06	333.16 ± 2.59	148.897 ± 2.69
Duve #5	80.0047962	23.989474	548.42	410.96 ± 2.82	137.461 ± 2.92
Error	±0.05 m	±0.05 m	±0.10 m	* interpolated values (see Sect. A)	

Table 2. Annual mean velocities for the period May 2008–2009 and May 2009–2010 based either on all available daily values (V_{mean}) or the first and last day's position at the beginning and end of the respective year (V_{be}). The velocity factor, V_{fac}, refers to current vs. previous year's V_{be}. At Basin-3, data is lacking between ~15 June–25 August, including both the pre-summer minimum and summer speed-up/maximum. The corresponding entry for V_{mean} is marked by a-superscript.

Stake (no.)	Period dd/mm/yyyy	Flow dir. (°azimuth)	V_{mean} (m a^{-1})	V_{be} (m a^{-1})	V_{fac}
B3 #1	04/05/2008–30/04/2009	72.99	415.6 ± 99.4	402.5	–
B3 #2	04/05/2008–30/04/2009	87.75	349.4 ± 65.5	348.3	–
B3 #3	05/05/2008–30/04/2009	98.47	264.9 ± 39.3	263.9	–
B3 #4	05/05/2008–30/04/2009	118.39	190.5 ± 25.5	189.7	–
B3 #5	05/05/2008–30/04/2009	119.50	118.1 ± 14.1	117.0	–
B3 #1	01/05/2009–30/04/2010	70.76	478.9 ± 86.3 [a]	485.1	1.21
B3 #2	01/05/2009–30/04/2010	86.91	444.1 ± 68.7 [a]	444.4	1.28
B3 #3	01/05/2009–30/04/2010	96.56	349.8 ± 48.7 [a]	349.6	1.32
B3 #4	01/05/2009–30/04/2010	116.64	256.3 ± 33.8 [a]	255.2	1.34
B3 #5	01/05/2009–30/04/2010	118.11	168.2 ± 23.6 [a]	165.3	1.41
Duve #1	01/05/2008–30/04/2009	295.50	198.8 ± 19.3	198.1	–
Duve #2	01/05/2008–30/04/2009	344.01	150.0 ± 12.5	149.4	–
Duve #3	01/05/2008–30/04/2009	357.08	111.1 ± 6.8	110.2	–
Duve #4	01/05/2008–30/04/2009	356.29	72.9 ± 7.7	71.6	–
Duve #5	01/05/2008–30/04/2009	345.65	35.8 ± 6.9	31.7	–
Duve #1	01/05/2009–26/04/2010	296.28	167.7 ± 11.1	174.1	0.88
Duve #2	01/05/2009–27/04/2010	341.63	147.2 ± 16.9	146.7	0.98
Duve #3	01/05/2009–27/04/2010	357.33	111.5 ± 11.0	110.7	1.00
Duve #4	01/05/2009–26/04/2010	355.89	74.1 ± 9.4	73.5	1.03
Duve #5	01/05/2009–04/05/2009	360.00	–	–	–

Table 3. Characteristics of the summer speed-up, following the pre-summer minimum in June, V_{JUN}, in terms of the onset date, timing and value of measured maximum velocities, V_{max}, and the normalized maximum flow enhancement relative to pre-summer velocities, V_{fac}.

Stake (no.)	V_{JUN} ($m\,a^{-1}$)	Onset (dd/mm/yyyy)	Summer max. (dd/mm/yyyy)	V_{max} ($m\,a^{-1}$)	V_{fac} (V_{max}/V_{JUN})
B3 #1	290.6 ± 8.8	09/07/2008	03/08/2008	698.5	2.40
B3 #2	253.2 ± 5.6	09/07/2008	03/08/2008	556	2.20
B3 #3	198.6 ± 3.7	13/07/2008	02/08/2008	374.1	1.88
B3 #4	149.0 ± 4.7	17/07/2008	02/08/2008	256.8	1.72
B3 #5	93.3 ± 6.4	20/07/2008	29/07/2008	143.2	1.53
Duve #1	178.0 ± 7.4	21/07/2008	03/08/2008	254.2	1.43
Duve #2	134.6 ± 6.2	28/07/2008	03/08/2008	190.2	1.41
Duve #3	105.0 ± 5.1	01/08/2008	01/08/2008	121.5	1.16
Duve #4	71.2 ± 7.6	–	–	–	–
Duve #5	37.8 ± 9.0	–	–	–	–
Duve #1	180.6 ± 10.2	–	–	–	–
Duve #2	150.7 ± 9.4	29/07/2009	04/08/2009	239.1	1.59
Duve #3	113.2 ± 8.6	31/07/2009	04/08/2009	163.8	1.45
Duve #4	74.8 ± 7.0	01/08/2009	04/08/2009	101.5	1.36
Duve #5	–	–	–	–	–

Title Page

Abstract | Introduction

Conclusions | References

Tables | Figures

|◀ | ▶|

◀ | ▶

Back | Close

Full Screen / Esc

Printer-friendly Version

Interactive Discussion
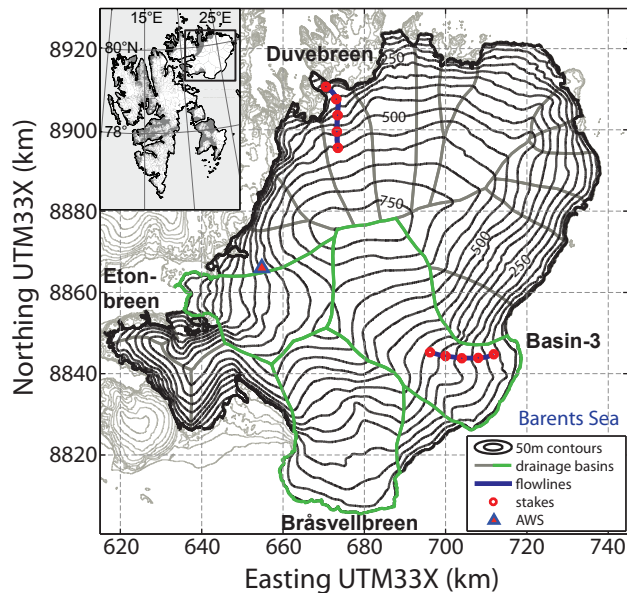
Fig. 1. Surface topography of Austfonna with 50 m elevation contours according to a new DEM by Moholdt and Kääb (2011). The black rectangle in the inset indicates the location within the Svalbard archipelago. Drainage basins are outlined in solid grey, in the case of the known surge-type basins in solid green. The survey routes along the central flowlines of Duvebreen and Basin-3 are marked in solid blue, the position of stakes with red dots and the AWS on Etonbreen with a triangle.
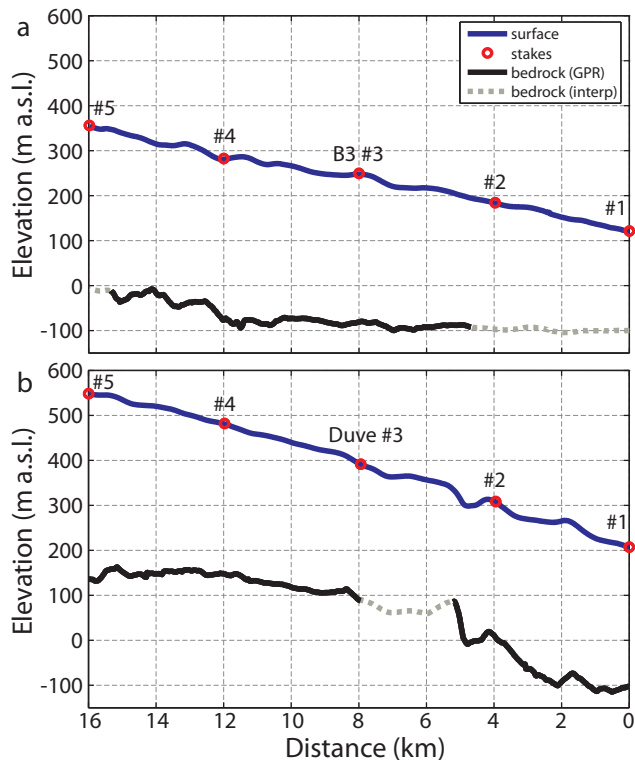
Fig. 2. Glacier geometry along central flowlines of Basin-3 **(a)** and Duvebreen **(b)**. Surface elevation (solid blue) in m a.s.l. is based on kinematic GPS measurements, GPR-derived ice thickness subtracted to yield bedrock elevation (solid black and dashed grey). Stake positions are marked with red dots.
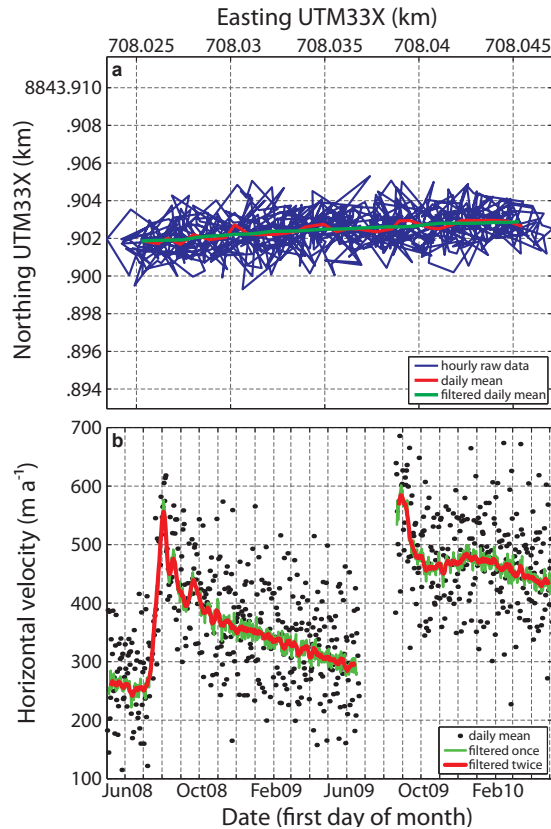
Fig. 3. Processing of continuous GPS observations. Positioning of stake Basin-3 #3 during June 2008 **(a)**: hourly GPS raw-data (blue), daily-mean values (red) and after application of a 7 day running mean (green). Flow velocities derived from displacement of GPS positions **(b)**, utilizing daily mean (black scatters) or 7 day filtered positions with/without additional 7 day filtering of the computed velocities (red/blue solid lines).
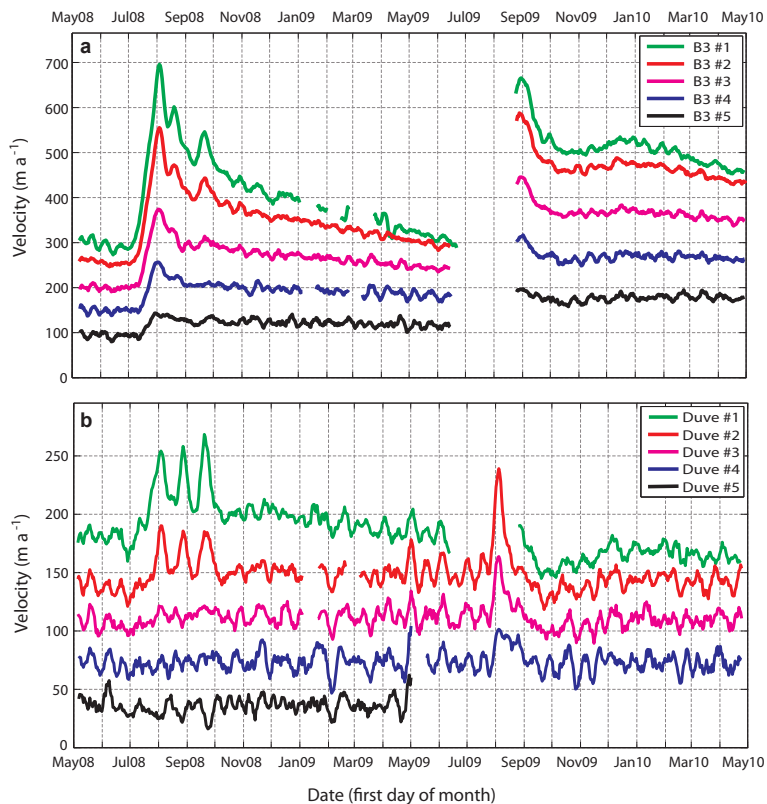
Fig. 4. Flow velocities along the central flowline of Basin-3 **(a)** and Duvebreen **(b)**, during May 2008–2010.
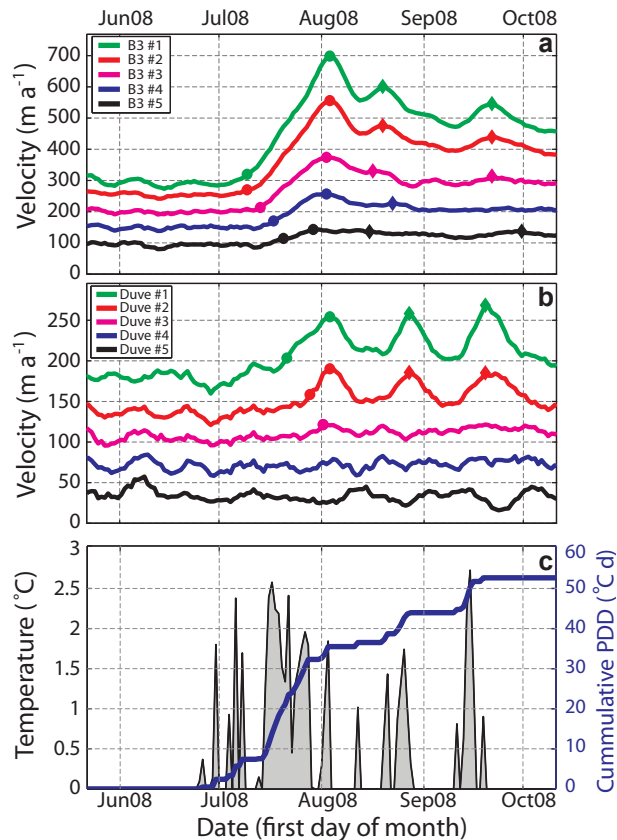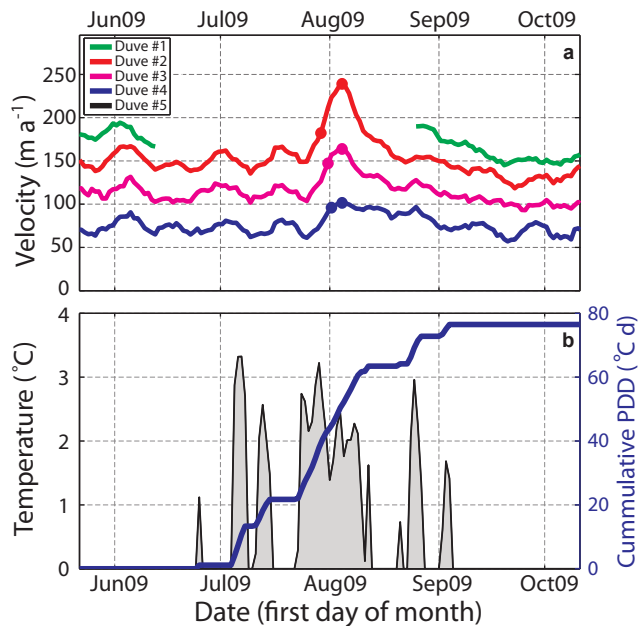
Fig. 5. Summer speed-up along the central flowline of Basin-3 **(a)** and Duvebreen **(b)** in summer 2008. Markers indicate the occurrence of the onset of summer speed-up and principle and secondary velocity peaks (see also Table 3). Positive daily mean air temperature and cumulative PDD at the AWS on Etonbreen is shown in **(c)**.

Title Page

Abstract | Introduction

Conclusions | References

Tables | Figures

|◄ | ►|

◄ | ►

Back | Close

Full Screen / Esc

Printer-friendly Version

Interactive Discussion

Fig. 6. Summer speed-up along the central flowline of Duvebreen in summer 2009 **(a)** with markers indicating the occurrence of onset of summer speed-up and peak velocity. Positive daily mean air temperature and cumulative PDD is shown in **(b)**.